Measurement of sub-surface core damage in sandwich structures using in-situ Hertzian indentation during X-ray computed tomography

S. Dietrich, M. Koch, P. Elsner, Kay A. Weidenmann

Angaben zur Veröffentlichung / Publication details:

Dietrich, S., M. Koch, P. Elsner, and Kay A. Weidenmann. 2014. "Measurement of sub-surface core damage in sandwich structures using in-situ Hertzian indentation during X-ray computed tomography." *Experimental Mechanics* 54 (8): 1385–93. https://doi.org/10.1007/s11340-014-9902-2.

Measurement of Sub-Surface Core Damage in Sandwich Structures Using In-situ Hertzian Indentation During X-ray Computed Tomography

S. Dietrich · M. Koch · P. Elsner · K. Weidenmann

Abstract Composite sandwich structures with honeycomb cores show varying properties in geometry and mechanical behavior depending on the studied scale. Herein a new test and evaluation method for sub-surface core damage in the indentation area of honeycomb sandwich structures using computed tomography is presented. The combination of X-ray micro-computed tomography (X-μCT) and an image analysis procedure adjusted to the detection of core deformation mechanisms allows the extraction and quantification of externally invisible, sub-surface damage in the sandwich composite. For this specific contact or indentation loading case on the sandwich face sheet an in-situ device is introduced, enabling a 3D analysis of the structural change during progressing indentation depth.

Keywords Micro-computed tomography · GFRP honeycomb sandwich · In-situ loading · Indentation · Contact modelling

Introduction

Down to the present day indentation and impact loading of composites and particularly sandwich structures has been investigated in experiments and represented through various models. Due to the fundamental difference of the mechanical response to local loading from bulk metallic materials the inherent micro- and meso-structure of composite materials has to be taken into account for design and material selection. Furthermore a detailed contact and deformation analysis in the interaction region between the composite surface and the indentor geometry has to be carried out to allow for a rigorous analytic or numeric description of the deformation. This is especially important since for honeycomb sandwiches the indentation and penetration of the face sheet is primarily influenced by the plastic crushing and buckling of the core walls and the related geometric aspects of the supporting core materials [1, 2]. The elastic deformation part can be readily described by high-order sandwich beam theory [3] or a 2D elasticity approach using Fourier series [4] which have been applied to describe the contact deformation and contact law in the vicinity of the indentation point based on assumptions of the contact geometry. Thereby the discrete cellular structure undergoes substantial strains and buckling phenomena coupled with large deformations and the formation of discontinuities due to rupture and disengagement of the periodic cell structure which need to be detected and correlated to the loading response of the structure. Yet only few investigations interconnect the modeling and failure mechanisms with experimental results and validate the deformation processes although several empirical assumptions are known in literature (see e. g. [5, 6]).

This contribution deals with the effects of static contact and indentation and their experimental visualization and characterization for sandwich composites. The authors present a novel experimental method aiming to extract the 3D damage characteristics and the damage extent near the indentation point including both the plastic collapse of the core and the deformation and rupture of the face sheet. The methods of damage characterization and recently the in-situ testing of composites using X-ray micro computed tomography (X-μCT) has evolved as a wide-spread tool in research and industry. The adaption of the method to special loading cases and multi-scale material structures still poses many difficulties for the interpretation and quantitative analysis of the 3D image data.

S. Dietrich (✉) · M. Koch · P. Elsner · K. Weidenmann
Institute for Applied Materials (IAM-WK),
Karlsruhe Institute of Technology, 76131 Karlsruhe, Germany
e-mail: stefan.dietrich@kit.edu

In engineering material science for example the investigation of damage in fiber reinforced composite laminates due to impact [7, 8] and the usefulness of X-μCT in the characterization of honeycomb structures and components was outlined [9, 10]. Furthermore the qualitative evaluation of such structures and their damage evolution has been the subject of comprehensive research activities to qualify the X-μCT methods in a wide area of micro-structural material characterization [11]. Hence we follow a similar approach in the acquisition of the tomographic data adjusted to the material combination and with a focus on a quantitative evaluation of damage parameters. Those parameters build the final characteristics which are used to explain and clarify the mechanical response of the sandwich composite.

In addition the adaption of mechanical in-situ testing to X-μCT has evolved from simple tension and compression loading [12] towards increasingly more complex load cases comprising bending [13] or crack growth. Simultaneously the evaluation of the deformation during loading in the form of 3D strain fields was improved through sophisticated digital volume correlation (DVC) algorithms and parallel computing capacities [14]. The recent development of these algorithms allows for the strain field on a scale where the materials image provides a compact yet heterogeneous gray value distribution to be determined. Therefore the DVC, like most microstructure tracking algorithms, can only be applied if a sufficiently noise-free and continuous gray value distribution originates from the micro-structure and choice of the imaging scale [15].

For a detailed description of the deformation mechanism and the collapse of cellular structures several problems in the application of the DVC method arise. The appropriate large scale for continuous gray values over a periodic cell structure which is still suppressing the image noise in the cell cavities conceals the microstructure at a cell scale completely [16]. It is therefore not suitable to give information on the large discontinuous deformations occurring with the anticipated snap through failure in cell wall buckling as provided for example by high resolution measurements in combination with morphological analysis of the cell structure [17]. Since the failure of a honeycomb core is due to the local collapse of several cells, in this work the approach was to detect the collapse failure zone without prior measurement of the elastic and vanishing plastic deformation in the single cell walls as would be resulting from a local DVC. The image processing steps will be presented in the following.

Experimentally the design and development of a special in-situ loading device for indentation and penetration deformation was necessary in order to incorporate the tomographic measurement into the standard testing procedure and to allow for a conclusive X-ray analysis. Recently the portfolio of available in-situ testing devices has been extended from tensile-compression loading [18] to bending [13, 19] and cyclic fatigue behavior [15]. To the knowledge of the authors impact or contact loading has not yet been exploited in an in-situ method although the qualitative control of the damage is a current topic of various material investigations [17, 7].

The microstructure scale of the sandwich composite varies across the sandwich components and is because of the already mentioned reasons difficult to resolve with DVC entirely. Therefore the honeycomb core failure under contact loading is the focus of this investigation. In this work an interrupted testing sequence is used to allow for a precise and fast measurement routine taking into account the loading conditions, the loading device and the composite component material behavior.

In this paper we present the testing method in detail, including the imaging techniques and X-μCT. Additionally the novel composite manufacturing method and the in-situ device are described. The experimental results comprise the carried out tests for two extremal material parameter combinations and the image evaluation data. The conclusion discusses the experimental results with respect to the damage and failure mechanisms and the possibility to achieve a concise analytical modelling of deformation and load history. Finally the accuracy and limits of the proposed methods are outlined and further advancements are discussed.

Materials and Manufacturing

PU Spraying of Honeycomb Sandwich Structures

The sandwich composites have been manufactured at the Fraunhofer Institute for Chemical Technology (ICT). The

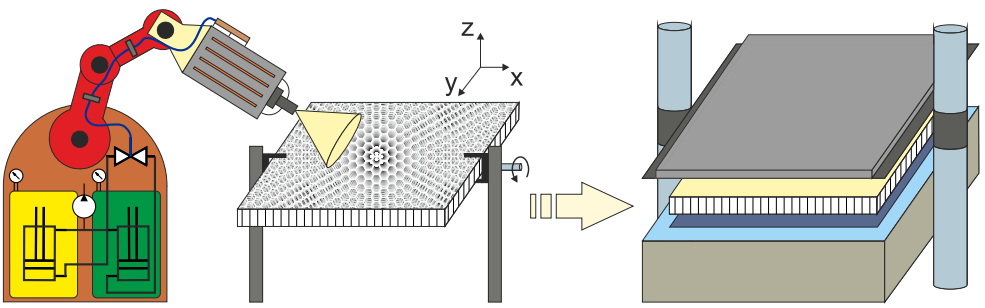

Fig. 1 Two step manufacturing process automated using a robot driven spraying and preform handling unit before the final pressing step in the mould

Table 1 Material properties measured in single component testing under compression (C) and tensile (T) loading conditions

	Core (C)	Face sheet (T) 450/600 g/m^2	PU matrix (T)
Young's modulus	145 MPa	12.3/13.6 GPa	3,106 MPa
Yield strength	2 MPa	168.5/216.7 MPa	64 MPa

manufacturing process can be divided into two steps. Therein the chopped strand mats (MA 141 - 300/450 from Glasseiden GmbH Oschatz) are completely impregnated with the PU (Baypreg/Desmodur from Bayer) and the sandwich preform is rotated around 180° treat both sides. In the second step the impregnated preform of face sheet and paper-board core (cell size 4.97 mm x 8.97 mm, wall thickness of 150 μm) is placed into a 600 kN mould carrier and the heated press carries out the compression of the face sheet and the curing of the matrix (see Fig. 1). A detailed description of the process and influential process or material parameters can be found in [20, 21]. In this work two combinations of process and material parameters expected to represent two extremal states for the mechanical response of the composite have been investigated. All the sandwiches had a total thickness of 20 mm determined by the pressing conditions. The first combination (S1) consists of a 450 g/m^2 face sheet and 1160 g/m^2 of PU as adhesive while the second combination (S2) has a 600 g/m^2 face sheet with a deposition of 479 g/m^2 of PU by the robot spraying head. For each combination 3 samples have been investigated to gain reassurance about the applicability of the new method and to account for manufacturing and material fluctuation.

Component mechanical properties

The mechanical properties of the components in the sandwich have been measured in single component tests under tension and compression according to the appropriate DIN standards (core compression/tension - DIN 53291/53292 [22, 23], face sheet tension - DIN 65469 [24], PU compression - DIN 844 [25]). The mean values of each testing series are depicted in Tab. 1 and provide the input parameters for the analytical modelling of the indentation process outlined in section 2.

Due to the focus on the herein developed in-situ testing device the measurement procedures and specific characteristics of the quasi-static component testing will not be discussed any further and the values provided here are only used to support the modelling of the sandwich structure and the usefulness of the testing method.

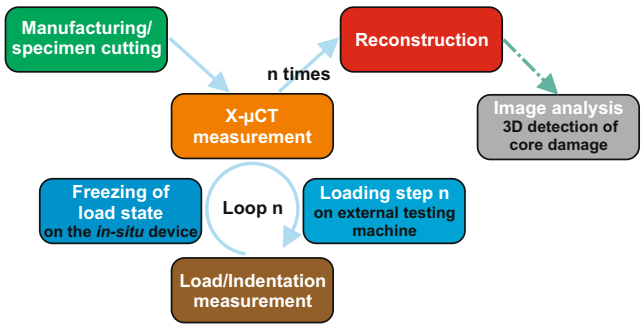

Fig. 2 Step sequence of indentation loading and X-μCT measurements leading to a 3D evaluation of the core damage development in a block diagram

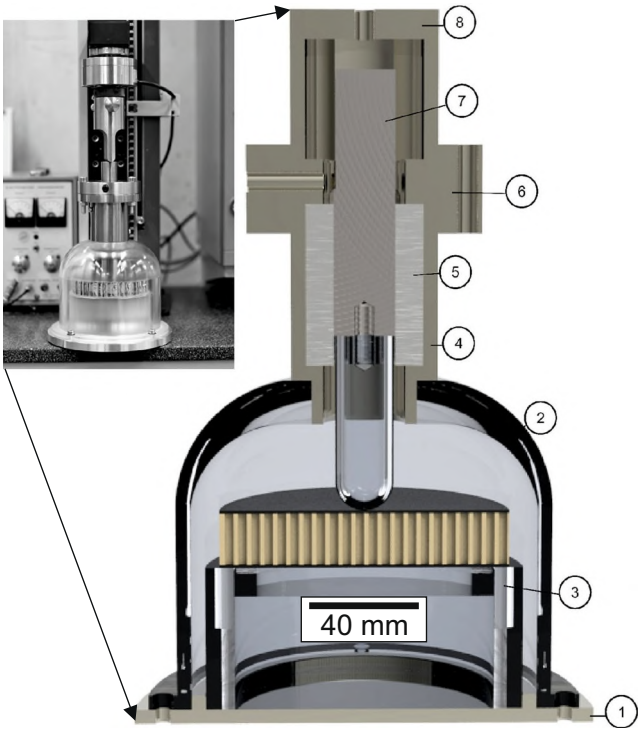

Fig. 3 Sectional view of the in-situ device including the sandwich sample below the PMMA indenter also indicating the base plate (**1**), bell shaped load frame (**2**), sample support (**3**), spline housing (**4**), spline hub (**5**), clamping ring (**6**), spline shaft with indenter (**7**) and closure head (**8**)

Experimental Procedure

In this section the experimental approach and the used devices are clarified and the design and development of

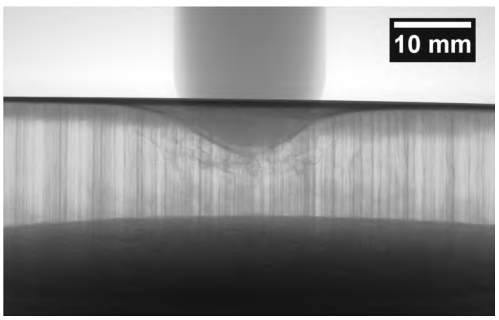

Fig. 4 Radiograph of a sandwich specimen in the in-situ apparatus with 6 mm penetration depth of the hemi-spherical PMMA indenter

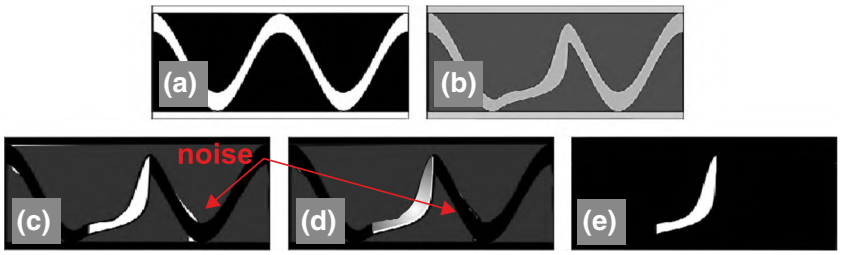

Fig. 5 Schematic of the steps applied to each image plane for the detection of lateral cell wall displacement

the new in-situ equipment and image analysis procedure are presented.

In Fig. 2 the overall course of measurement is illustrated. At first the sandwich plates are cut into circular samples using a diamond-tipped hole-cutting drill bit with a diameter of 100 mm. Subsequently the samples are mounted into the in-situ fixture to be fed into the measuring loop. A first X-μCT measurement is carried out without loading the sample to capture the intact state of the sample. In the first loading step the in-situ device is placed on a Zwick universal testing machine with a 2.5 kN load cell and a inductive displacement transducer to apply the predefined indentation. During the indentation movement the load and displacement history is recorded. As last step before the next X-μCT measurement the load state is frozen by a clamping fixture holding the indenter into position during X-μCT data acquisition. For each X-μCT measurement a subsequent chain of reconstruction and image analysis is carried out in parallel and provides the final results for the failure behaviour of the sandwich samples. The three main steps are depicted in the following.

In-situ indentation device

The in-situ device was designed under two main aspects. On the one hand the disturbance of the image quality through the load frame and indenter has to be minimized. On the other hand the load carrying parts have to withstand the occurring forces with minimized creep and elastic deformation during the x-ray acquisition. Therefore an approach with a mixture of materials and shapes has been chosen to comply with these restrictions. The sectional view in Fig. 3 depicts the components of the apparatus. The main components therein are the bell shaped load frame out of PMMA with wall diameter of

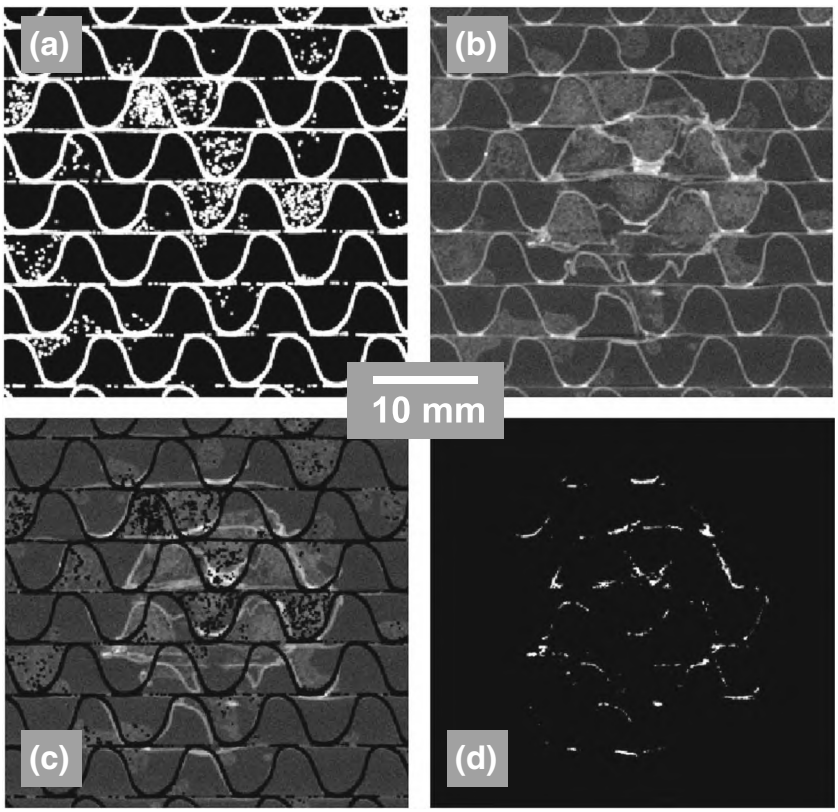

Fig. 6 Steps in the image processing of a single image plane of configuration S2 with the binarized intact sample (**a**), gray-valued damaged sample (**b**), the inverse multiplication of both (**c**) and the final distance transformed and binarized image indicating the displaced cell walls (**d**)

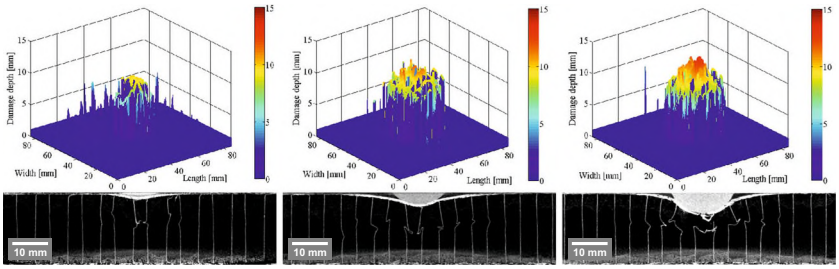

Fig. 7 Failure surface and median slice of indentations at 2, 4 and 6 mm for a sample of configuration S2

15 mm adjusted for a maximum load capacity of 5 kN and geometrically optimised for minimal creep during the measurement time. A simplified calculation of the load frame strength was carried out by representing the shape as a closed cylinder with a drilled hole on top. This conservative approximation provided an estimate of the maximum deflection of the indenter of 0.4 mm according to a bending stress of 21 MPa in the PMMA frame well below the yield strength of 115 MPa. The sample base plate was as well made from PMMA in the form of a compact cylinder with a height adjusted to allow the penetration of X-rays contributing to the radiography along a homogeneous path through the bell jar transmitting the load. The hemispherical indenter contacting the sample was machined out of PMMA to avoid the occurrence of metal artefacts in the final reconstructed image data. It was then screwed in a steel spline shaft guided by a spline hub attached to a steel housing on the load frame. A clamping device with three ball head screws was integrated into the housing, allowing to fix the indenter in its position with minimum abrasion of the shaft and sufficient friction force to stabilize and hold the reaction forces of the sample contact.

Computed Tomography

In this research project a laboratory tomography scanner (YXLON Precision) has been used. The X-ray tube has been operated at an acceleration voltage of 100 kV and a target current of 30 μA. The in-situ device has been mounted on the rotary table using a center hole and was rigidly fixed to the table to avoid movement. During the rotation of the turntable with an angular increment of 0.18° over 360° the intensity of X-ray transmission was recorded using a Perkin Elmer XRD1620 AN flat panel detector with a pixel size of 200 μm and a total field of view of 2048 × 2048 pixel. The geometrical magnification was chosen to resolve the cellular structure of the honeycomb sandwich with a resolution of 48 μm while still retaining the entire sample as region of interest. For the projections the detector integration time was 1 s with an projection binning of 2 projections at each rotation angle for noise reduction.

Image analysis procedure

The obtained projections (see Fig. 4) have been reconstructed using a standard Feldkamp filtered back-projection algorithm [26] to generate the 3D volume data

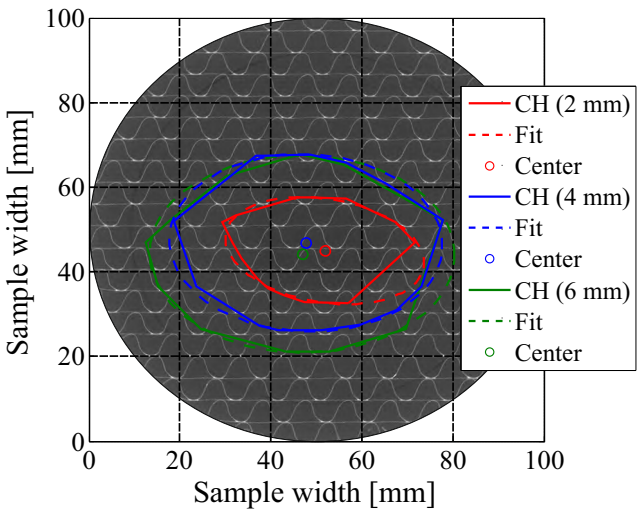

Fig. 8 Projected lateral damage extent for the three indentation states (2–6 mm) of Fig. 7 indicating the convex hull (CH) as well as the fitted equivalent ellipses with their center points for a sample of configuration S2

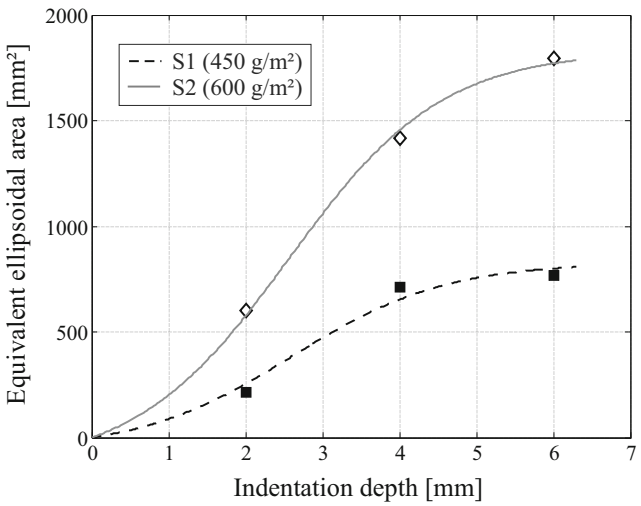

Fig. 9 Mean values of the ellipsoidal equivalent area of 3 samples in each configuration (S1 and S2) for increasing indentation depths

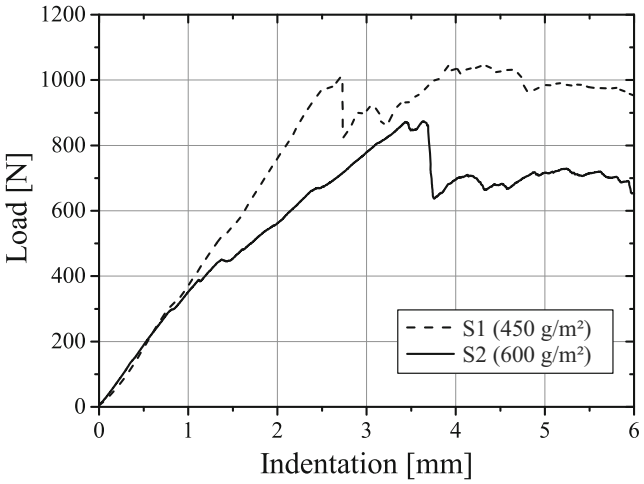

Fig. 10 Comparison of typical load vs. indentation curves for the two investigated configurations indicating the higher energy absorption and maximum load of S1 and the stiffness drop of S2

(voxel data) representing the linear attenuation coefficient of the samples microstructure.

Subsequently the image data was cropped and registered to the intact first reference measurement using the commercial software VGStudio Max 2.1 (Volume Graphics, Heidelberg, Germany). The aligned images were then fed into an imaging pipeline of morphological image filters (see e. g. [27]) using the image analysis software ImageJ [28] acting on each image plane along the thickness direction of the sample to detect the lateral displacement of the cell walls. This pipeline comprised the binarization (Otsu threshold [29]) of the intact (Fig. 5(a)) and deformed (Fig. 5(b)) image followed by a voxel-wise logical NOT-AND operation. In this logical operation step each voxel in the intact image was inverted (NOT operation) and multiplied with the respective voxel in the deformed image (AND operation) which leads to a binary image of only the deformed parts of the imaged wall structure (see Fig. 5(c)). While the registration of the images at different load steps can be carried out with a high precision showing only pixel-wise deviations in the overlap of the cell geometry for undamaged regions, the subsequent morphological operations are prone to image noise. Therefore after removing the initial structure from the image data this noise has to be removed by an additional distance transform (see Fig. 5(d)) and thresholding step (see Fig. 5(e)) allowing only displacements larger than one pixel into the evaluation process.

The schematic of the stepwise changes in the image data during image processing are outlined in Fig. 5 and show the intermediate results and final step to detect the lateral displacement of the cell walls. A detailed description of the single algorithms can be found in textbooks on image processing like e.g. [30].

The combination of detected cell wall displacements provides a hull for the region of the sample where core failure occurred. For a concise representation of this failure zone the maximum depth of the core damage from the side of the indented face sheet is sampled and translated into a scatter plot for further statistical and geometrical investigation in the form of enveloping 3D surfaces.

Results and Discussion

Results

The application of the image processing steps on the 3D data sets is indicated in Fig. 6. In this interior slice (≈ 10 mm below the face sheet) the importance of the multiplication and thresholding step is apparent. For an automatic and objective choice during the thresholding procedures the Renyi entropy measure [31] provided by the ITK imaging library [32] was applied.

The image of the displaced cell walls can easily be displayed in a 3D surface plot as indicated in the image series in Fig. 7. Therein the growing lateral extent apparent from the steep drop to zero indentation depth can be estimated very precisely. Additionally the change in depth for rising indentation is visible through the maximum value of the peak surface (see Fig. 7).

For a clearer and measurable visualization of the damage extent the lateral dimensions of the surface damage can be presented in the form of a convex hull. This convex hull of all the exterior cell points in the sample plane provides the possibilityto measure the projected damage area beneath the face sheet in a ellipse fit (see Fig. 8). A closer look at the shape of the convex hull clearly shows an anisotropy in the damage development and failure zone shape determined by the geometric anisotropy of the honeycomb cell.

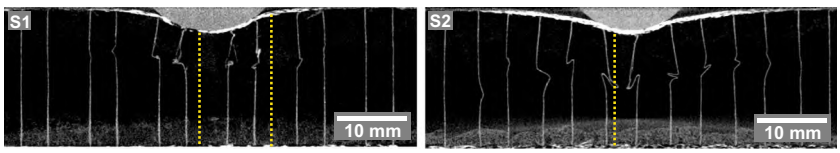

Fig. 11 Comparison of the median slice after 2 mm indentation for configuration S1 (left) and S2 (right) with clearly visible different extent of cell wall buckling and lines indicating the rupture points of the face sheets

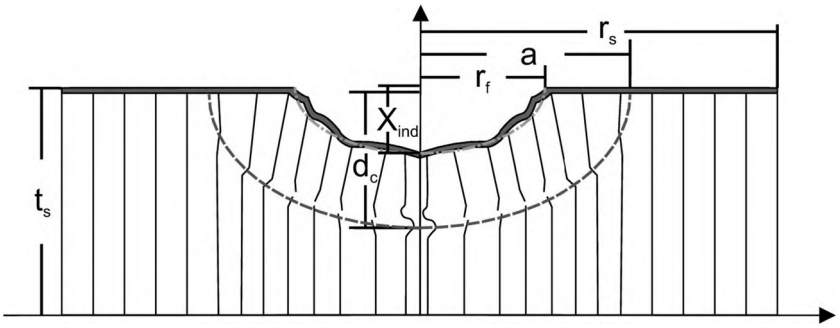

Fig. 12 Schematic of the damage zone indicating face sheet indentation and distributed cell wall buckling failure in the honeycomb core

For the two investigated configurations the according area of the equivalent ellipse is plotted in Fig. 9 and shows approximately a trend of a S-curve. The eventual plateau is strongly connected to the point of face sheet rupture. From this point on further indentation of the indentor ceases to cause a rising bending curvature of the face sheet into the core material whereupon no additional cell deformation is induced. The investigated sample configurations distinguish mainly in the size of the area and the indentation depth where this saturation of the rising area size occurs.

Accordingly the load vs. indentation curves show a very early decrease in stiffness at an indentation of 1.38 ± 0.17 mm for the S2 configuration coinciding with the first buckling honeycomb cell walls (see Fig. 10). The total energy absorption up to 6 mm determined from the integral of the load vs. indentation curve is 4.326 ± 0.239 J for S1 and 3.389 ± 0.096 J for S2.

Discussion

The results show clearly the possibility to detect honeycomb core damage during the indentation history with the in-situ device. The approach in this work to use simple image processing techniques to quantify the damage extent in the core in direct correlation with de load-deflection curve can finally be used to detect and explain the dominant damage mechanisms. The limiting factors in the evaluation using these imaging techniques lie in the X-μCT measurements with the relatively low resolution of 48 μm in comparison to the cell wall thickness of only 150 μm. Additionally through the distance transform step with subsequent thresholding the displacement of deformed cell walls can only be determined if larger than or equal to twice the resolution limit. The natural way to overcome this problem by reducing the sample size however is infeasible due to the lateral extent of the damage zone as indicated in Fig. 8 which forbids smaller samples if the entire damage should be covered in one sample.

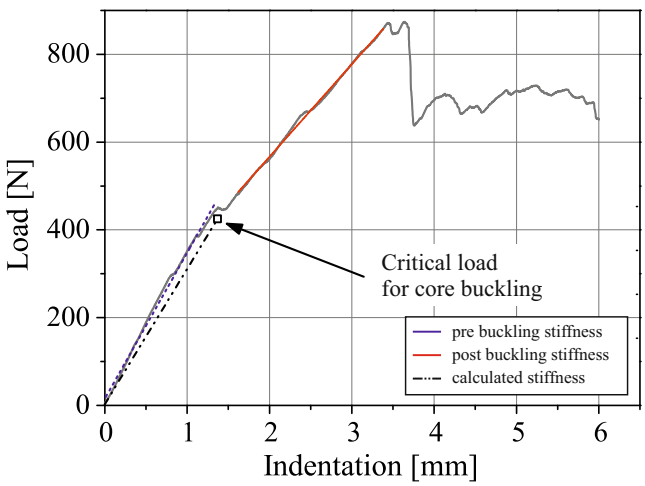

Fig. 13 Experimental static indentation curve from in-situ testing (configuration S2) and estimate of the critical buckling load using [5, 6] with the determined failure zone from the image processing steps

Comparing the development of the damage areas beneath the face sheet it is particular, that samples with lower face sheet weight (S1) of 450 g/ m^2 show a around 100 N higher sustained peak load and over 0.5 J higher energy absorption in theload history than the heavier face sheets (S2) of 600 g/ m^2. Especially since the extent of the damage zone for S1 is significantly lower than for S2 those two parameters were expected to be in reverse order. The possible explanation for this observed damage behaviour can be given through the higher membrane strength and stiffness of the thicker face sheet configuration S2. Therein the tensed face sheet undergoes a smaller curvature under the pressure of the hemispherical indenter and therefore creates a larger core damage through the non aligned load on a higher amount of cell walls (see Fig. 11 right).

Through this damage in the supporting cell walls the energy absorption of the core and the maximum load of the face sheet before rupture are significantly decreased. It is therefore a specific property of the configuration S1 with small membrane bending to only locally divert the cell walls and allow for a high curvature with higher peak load. This is then in return connected to the build up of columnar separation of the face sheet and core under the indenter which accounts for the still high energy absorption after face sheet rupture because the collapse of the cut free column provides a higher resistance for the penetration of the indenter than the common petal shaped fracture of the face sheet observed in the S2 configuration.

Apart from providing the micro-structural background for the penetration mechanism the image processing results are of particular interest for the description of elasto-plastic deformation at first contact between sandwich and indenter. The application of the results in the previous section for a detailed description of the sandwich composite behaviour and the possible incorporation into a analytical modelling procedure can be realized for the configuration S2 using standard numeric software like Matlab®. Based on the approaches in [5, 6], which comply with the deformation behaviour present in configuration S2, we use a comprehensive database of material properties measured for the sandwich components (see Sec. 2) to predict the load of first core damage. With the tomography based geometric measures for the failure zone depicted in Fig. 12 the supporting core area (see Fig. 9) is realistically implemented into the equations for the critical core damage load.

This is of utmost importance for sandwich composites with weak and thin face sheets and therefore a lack of bending stiffness to support the indentation load. Through the correction of the dependence between the radius of the supporting core area and the indentation depth of the indenter after [33] the new equivalent support radius can be expressed using a fit to the S-curves of Fig. 9.

$$a = \sqrt{\frac{3K_0 X_{ind}}{2\pi q}} \Leftrightarrow S{-}curves: \; a_{eq} = \sqrt{\frac{A}{\pi^2 (B + e^{-X_{ind}})} + C}. \tag{1}$$

Using the fit to the experimental contact data with parameters A, B, and C (Fig. 9) it is possible to predict the observed core damage initiation load with only 5 % deviation as can be seen in Fig. 13. Compared to the calculation without precise information about the contact geometries this is an improvement of 10 %.

An implication of fitting an empirical model through the testing and evaluation procedure described in this work is the further need to find a physical basis for the fit parameters and correlate them to damage mechanisms not yet revealed. Yet the assumptions of perfectly plastic cores and membrane stretching as well as face sheet bending are rather approximate for realistic materials and we therefore consider the gain in precision as a valuable aspect in the sandwich modelling.

Conclusion

In this paper we present an innovative experimental and analysis procedure to investigate the compression collapse of honeycomb cores in sandwich structures under indentation loading. This procedure is carried out during X-μCT scanning while the indentation load is applied to the sample. The development of an according innovative in-situ indentation device for X-μCT measurements of laminated or sandwich composites was presented with a loading capacity of 5 kN and a direct interface to a standard testing machine through an interrupted testing scheme. The results from the testing setup in form of load–displacement curves and 3D image data of the loaded sample could be inserted into an imaging pipeline providing the geometric properties of the indentation surface and core failure zone. These results allow for a deeper insight into the core damage mechanisms and the relation to the honeycomb cell geometry. Finally these extracted quantitative informations could be implemented into an analytical model of the sandwich composite and provided an increase in precision for the prediction of cell buckling effects on the loading history of the sandwich structure.

Acknowledgments The authors wish to thank Dr.-Ing. Jan Kuppinger for manufacturing and providing the sandwich composite panels investigated herein.

These investigations were carried out through the research activities of the KITe hyLITE Plus project. This project is funded by the European Union through the program European Funds for Regional Development as well as state government of Baden-Württemberg in Germany.

References

1. Olsson R, McManus HL (1996) Improved theory for contact indentation of sandwich panels. AIAA J 34(6):1238–1244
2. Olsson R (2002) Engineering method for prediction of impact response and damage in sandwich panels. J Sandw Struct Mater 4(1): 3–29
3. Petras A, Sutcliffe M (1999) Indentation resistance of sandwich beams. Compos Struct 46(4):413–424
4. Swanson SR, Kim J (2003) Design of sandwich structures under contact loading. Compos Struct 59(3):403–413
5. Foo CC, Chai GB, Seah LK (2008) A model to predict low-velocity impact response and damage in sandwich composites. Compos Sci Technol 68(6):1348–1356
6. Foo CC, Seah LK, Chai GB (2008) Low-velocity impact failure of aluminium honeycomb sandwich panels. Compos Struct 85(1):20–28
7. Tan K, Watanabe N, Iwahori Y (2011) X-ray radiography and microcomputed tomography examination of damage characteristics in stitched composites subjected to impact loading. Compos Part B 42(4):874–884
8. Bull D, Helfen L, Sinclair I, Spearing S, Baumbach T (2013) A comparison of multi-scale 3d x-ray tomographic inspection techniques for assessing carbon fibre composite impact damage. Compos Sci Technol 75:55–61
9. Davies P, Choqueuse D, Bourbouze G (2011) Micro-tomography to study high-performance sandwich structures. J Sandw Struct Mater 13(1):7–21
10. T. Liu, A.A. Malcolm, J. Xu, in 2nd International Symposium on DNT in Aerospace 2010 (2010)
11. Dietrich S, Weidenmann K, Elsner P (2014) 3d tomographic characterization of sandwich structures. NDT & E International 62:77–84
12. Bay BK (2008) Methods and applications of digital volume correlation. The J of Strain Analysis for Engineering Design 43(8):745–760

13. Forsberg F, Sj¨odahl M, Mooser R, Hack E, Wyss P (2010) Full threedimensional strain measurements on wood exposed to three-point bending: Analysis by use of digital volume correlation applied to synchrotron radiation micro-computed tomography image data. Strain 46(1):47–60
14. M. Gates, J. Lambros, M.T. Heath (2011) Towards high performance digital volume correlation, Experimental Mechanics 51(4), 491–507 26 Stefan Dietrich et al
15. Limodin N, Rthor J, Buffire JY, Hild F, Roux S, Ludwig W, Rannou J, Gravouil A (2010) Influence of closure on the 3d propagation of fatigue cracks in a nodular cast iron investigated by x-ray tomography and 3d volume correlation. Acta Mater 58(8):2957–2967
16. Roux S, Hild F, Viot P, Bernard D (2008) Three-dimensional image correlation from x-ray computed tomography of solid foam. Compos A: Appl Sci Manuf 39(8):1253–1265
17. Viot P, Plougonven E, Bernard D (2008) Microtomography on polypropylene foam under dynamic loading: 3d analysis of bead morphology evolution. Compos A: Appl Sci Manuf 39(8):1266–1281
18. Buffiere JY, Maire E, Adrien J, Masse JP, Boller E (2010) In situ experiments with x ray tomography: an attractive tool for experimental mechanics. Exp Mech 50(3):289–305
19. Brault R, Germaneau A, Dupr J, Doumalin P, Mistou S, Fazzini M (2013) In-situ analysis of laminated composite materials by x-ray microcomputed tomography and digital volume correlation. Exp Mech 53(7):1143–1151
20. Kuppinger J, Weidenmann K, Kordick M, Wafzig F, Henning F, Elsner P (2010) Influence of fibre length and concentration on the mechanical properties of long glass fibre reinforced polyurethane. J of Plastics Technology 5:205–227
21. Kuppinger J, Weidenmann K, Haspel B, Wafzig F, Hennig F, Elsner P (2011) Influence of processing conditions, fiber contents and fiber lengths on fiber orientation in the polyurethane fiber spraying process. J of Plastics Technologies 6:44–65
22. DIN 53291 - Druckversuch senkrecht zur Deckschichtebene (1982)
23. DIN 53292 - Zugversuch senkrecht zur Deckschichtebene (1982)
24. DIN 65469 - Faserverst¨arkte Kunststoffe - Zugversuch an einlagigen Zugflachprobek¨orpern (1992)
25. DIN 844 - Harte Schaumstoffe - Bestimmung der Druckeigenschaften (2009)
26. Feldkamp LA, Davis LC, Kress JW (1984) Practical cone-beam algorithm. J Opt Soc Am A 1(6):612–619
27. B. J¨ahne, Image processing for scientific applications (CRC press Boca Raton, 1997)
28. Schneider CA, Rasband WS, Eliceiri KW et al (2012) Nih image to imagej: 25 years of image analysis. Nat Methods 9(7):671–675
29. Otsu N (1975) A threshold selection method from gray-level histograms. Automatica 11(285–296):23–27
30. B. J¨ahne, Digitale Bildverarbeitung (Springer DE, 2005)
31. Sahoo P, Wilkins C, Yeager J (1997) Threshold selection using renyi's entropy. Pattern Recogn 30(1):71–84
32. T.S. Yoo, M.J. Ackerman, W.E. Lorensen, W. Schroeder, V. Chalana, S. Aylward, D. Metaxas, R. Whitaker (2002), Engineering and algorithm 28 Stefan Dietrich et al. design for an image processing api: a technical report on itk-the insight toolkit, Studies in Health Technology and Informatics pp. 586–592
33. Zhou D, Stronge W (2006) Low velocity impact denting of {HSSA} lightweight sandwich panel. Int J Mech Sci 48(10):1031–1045